Impact of variable fluid properties on forced convection of Fe_3O_4-CNT/water hybrid nanofluid in a double-pipe mini-channel heat exchanger

Amin Shahsavar[1], Ali Godini[1], Pouyan Talebizadeh Sardari[2], Davood Toghraie[3,*]

[1] Department of Mechanical Engineering, Kermanshah University of Technology, Kermanshah, Iran

[2] Fluids and Thermal Engineering Research Group, Faculty of Engineering, The University of Nottingham, University park, Nottingham, United Kingdom

[3] Department of Mechanical Engineering, Khomeinishahr Branch, Islamic Azad University, Isfahan, Iran

Abstract

The objective of this study is to assess the hydrothermal performance of a non-Newtonian hybrid nanofluid with temperature-dependent thermal conductivity and viscosity compared with a Newtonian hybrid nanofluid with constant thermophysical properties. A counter-current double-pipe mini-channel heat exchanger is studied to analyze the effects of hybrid nanofluid. The nanofluid is employed as the coolant in the tube side while the hot water flows in the annulus side. Two different nanoparticles including Tetra Methyl Ammonium Hydroxide (TMAH) coated Fe_3O_4 (magnetite) nanoparticles and Gum Arabic (GA) coated Carbon Nanotubes (CNTs) are used to prepare the water based hybrid nanofluid. The results demonstrated that the non-Newtonian hybrid nanofluid always has a higher heat transfer rate, overall heat transfer coefficient, effectiveness, and performance index than those of the Newtonian hybrid nanofluid, while the opposite is true for pressure drop and pumping power. Supposing that the Fe_3O_4-CNT/water hybrid nanofluid is a Newtonian fluid with constant thermal conductivity and viscosity, leads to a large error in the

*Corresponding author
E-mail address: toghraee@iaukhsh.ac.ir

computation of pressure drop (1.5-9.71%), pumping power (1.5-9.71%), and performance index

of heat exchanger (1.86-11.25%), whereas the errors in the computation of heat transfer rate,

overall heat transfer coefficient, and effectiveness aren't considerable (less than 2.91%).

1. Introduction

Double-pipe heat exchangers have been widely employed in various applications to exchange heat

between two fluids called as heat transfer fluids [1, 2]. They are an essential part of almost all the

industries, including the oil and gas industry, power generation, refrigeration, and nuclear power.

Due to the great importance of heat exchangers, improving their efficiency is a very important

issue. So far, several methods have been proposed in the literature to enhance heat exchanger

performance such as using various fins and turbulators. However, these modifications offer several

disadvantages like increase in pressure drop, weight and volume of heat exchangers that limit their

usage.

Over the past decade, scientists and researchers around the world have revealed that the heat

exchanger performance can be considerably enhanced by improving the thermal conductivity of

working fluids [3, 4]. This goal can be achieved through the use of nanofluids, which are prepared

by suspending nanoparticles with sizes typically of 1-100 nm in conventional heat transfer fluids

such as water, oil, and ethylene glycol [5-8]. This term was first suggested by Choi [9] in 1995,

and it has since gained in popularity [10-17].

A great number of experimental and numerical works have been performed on the various aspects of different nanofluids performance in double-pipe heat exchangers [18-22]. Maddah et al. [23] experimentally evaluated the effects of Al_2O_3-water nanofluid on the performance of a horizontal double-pipe heat exchanger under turbulent flow regime and showed 52% and 12% enhancements in the friction factor and heat transfer rate, respectively. Mousavi et al. [24] numerically studied the effect of a variable magnetic field on the hydrothermal characteristics of Fe_3O_4-water nanofluid flowing through a sinusoidal double-pipe heat exchanger and reported the enhancement of Nusselt number in the presence of magnetic field. Saeedan et al. [25] numerically examined the effect of Cu-water, CuO-water and CNT-water nanofluids on the performance of a finned type heat exchanger. They found that both the Nusselt number and pressure drop intensify with increasing nanoparticle concentration. Sarafraz et al. [26] experimentally studied the use of CNT-water nanofluid inside a double-pipe heat exchanger. They assessed the impact of different effective parameters on the convective heat transfer coefficient in laminar and turbulent flow regimes and found that the proposed nanofluid can enhance the heat transfer by almost 44% compared with the pure water. Kumar et al. [27] experimentally surveyed the effect of Fe_3O_4-water nanofluid on the performance of a double pipe heat exchanger with a longitudinal fin with return band under turbulent flow regime. They showed the enhancement of Nusselt number with increasing the Reynolds number and nanoparticle concentration. Hussein [28] experimentally examined the flow of Aluminum Nitride- ethylene glycol nanofluid through a double-pipe heat exchanger and showed the increase of Nusselt number with increasing the flow rate and volume concentration of nanofluid. Shirvan et al. [29] studied the influence of Reynolds number and nanoparticle concentration on the performance of Al_2O_3-water nanofluid inside a double-pipe heat exchanger

67 and showed the enhancement of Nusselt number with increasing the Reynolds number and

68 decreasing the nanoparticle concentration.

69 To enhance the rate of heat transfer, hybrid nanofluids has attracted lots of attention using a

70 combination of different nanoparticles in the nanofluids in order to take the advantage of them

71 [30-36]. Esfe et al. [37] experimentally studied the thermal conductivity of ethylene glycol based

72 hybrid nanofluid containing ZnO-CNT nanoparticles. They showed the improvement of thermal

73 conductivity using ZnO and CNT nanoparticles compared with the base fluid and developed a new

74 correlation for the calculation of thermal conductivity based on the experimental data using an

75 artificial neural network (ANN).

76 The combination of Fe_3O_4 with CNT nanoparticles is widely used as a promising hybrid nanofluid.

77 Baby and Sundara [38] studied the effects of nanoparticles concentration on the thermal

78 conductivity of Fe_3O_4-CNT/water hybrid nanofluid and reported 6.5-10% improvement in the

79 thermal conductivity of nanofluid in the temperature range of 30-50 °C compared with the base

80 fluid. Felicia and Philip [39] investigated an oil-based Fe_3O_4-CNT hybrid nanofluid in the presence

81 of a magnetic field and showed the enhancement of viscosity with increasing magnetic field

82 intensity. Sundar et al. [40] experimentally assessed the hydrothermal characteristics of Fe_3O_4-

83 CNT/water hybrid nanofluid in a circular tube and presented 14.8% improvement in the Nusselt

84 number using nanofluid with concentration of 0.3% at Reynolds number of 3000. Shahsavar et al.

85 [41] studied the use of Fe_3O_4-CNT/water hybrid nanofluid in a heated tube in the presence of both

86 constant and alternating magnetic fields. They showed higher improvement of heat transfer using

87 a constant magnetic field compared with an alternating one. Harandi et al. [42] conducted

88 experiments to determine the thermal conductivity of Fe_3O_4-CNT/EG hybrid nanofluid at different

89 temperatures and found the improvement of thermal conductivity with increase in temperature and

90 nanoparticle concentration.

91 In most of the previous research works on the performance of heat exchangers containing various

92 nanofluids, the thermophysical properties of the nanofluid have been assumed as constant and the

93 nanofluid itself has been considered as Newtonian [43, 44]; while various studies have shown that

94 the thermophysical properties of nanofluids are a function of temperature, and that the majority of

95 nanofluids exhibit a non-Newtonian behavior [45-47]. In this research, we want to see if a

96 significant difference is observed in the performance parameters of a heat exchanger (i.e. pumping

97 power, effectiveness, and performance index) by assuming constant properties and a Newtonian

98 nature for nanofluids. We also want to find out: under what conditions the assumptions of constant

99 properties and Newtonian nature of nanofluid can be used in the analysis of heat exchangers? This

100 is done by comparing the performance parameters of a counter-current double-pipe heat exchanger

101 containing Newtonian Fe_3O_4-CNT/water nanofluid of constant properties with the performance

102 parameters of a heat exchanger containing the non-Newtonian Fe_3O_4-CNT/water hybrid nanofluid

103 with temperature dependent thermal conductivity and viscosity, at different Reynolds numbers and

104 concentrations.

105

106 **2. Physical properties of nanofluid**

107 This investigation is conducted on a hybrid nanofluid consisting of TMAH coated magnetite

108 nanoparticles and GA coated CNTs. It was prepared by mixing different volume ratios of Fe_3O_4-

109 water nanofluid and CNT-water nanofluid, followed by 5 min sonication [48]. The detailed

110 description of the preparation method can be found in Refs. [48-50]. The magnetite and CNT

111   nanoparticles are attached physically because of interaction between the molecules of TMAH and

112   GA.

113   After careful preparation and characterization, a series of experiments were performed to evaluate

114   the thermophysical properties of the hybrid nanofluid. The hybrid nanofluid shows the non-

115   Newtonian and Newtonian behaviors at low (up to 70 s^{-1}) and high shear rates, respectively.

116   Additionally, the viscosity of the hybrid nanofluid enhances with increase in volume concentration

117   of nanoparticles, while reduces with increasing the temperature. However, the thermal

118   conductivity increases with temperature and volume concentration.

119   Based on the data obtained from experiments, the artificial neural network (ANN) was used to find

120   a correlation between the thermal conductivity and temperature and volume concentration of Fe_3O_4

121   and CNT nanoparticles [51]. For the viscosity, a correlation is developed as a function of

122   temperature, shear rate, and volume concentrations of Fe_3O_4 and CNT nanoparticles [51]. The

123   acquired neural network models illustrate a good accuracy to predict the thermal conductivity and

124   viscosity according to Fig. 1. The correlations developed are presented in appendix A, and it is

125   clear that the models are temperate dependent.

126
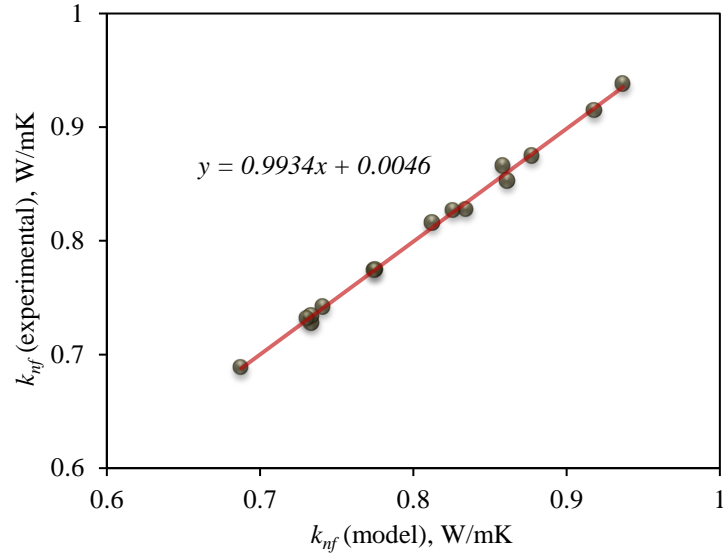
(a)
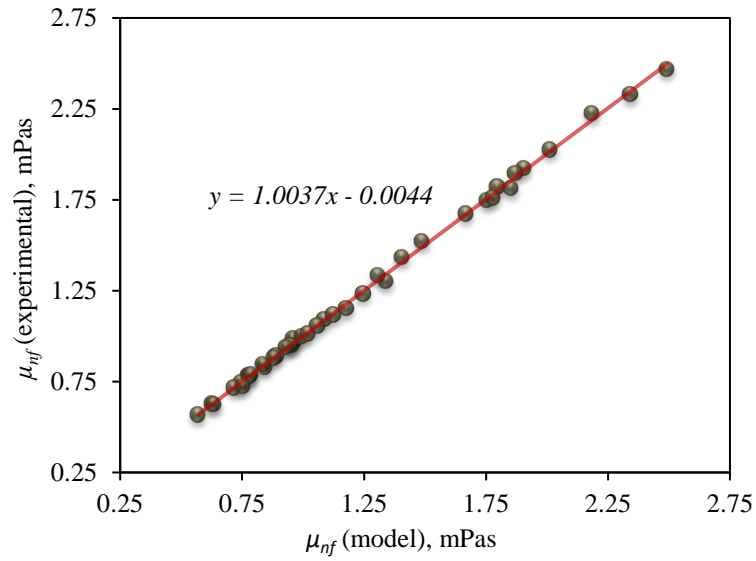
(b)

Fig. 1. Results obtained from the developed models in comparison with the experimental data: (a) thermal conductivity, (b) viscosity [18].

127

128   The viscosity and thermal conductivity of the considered Newtonian hybrid nanofluids are

129   reported in Table 1. The considered viscosity for the Newtonian nanofluid is equal to the viscosity

130   of the non-Newtonian nanofluid at the same concentrations of CNT and magnetite nanoparticles

131   at shear rates higher than 70 s⁻¹. Also, the considered thermal conductivity for the Newtonian

132   nanofluid samples is the same as the thermal conductivity of the non-Newtonian nanofluid at the

133   inlet temperature of nanofluid.

134

Table 1. Characteristics of the studied Newtonian nanofluid samples.

	φ_{CNT} (%) = 0.1%					φ_{CNT} (%) = 1.35%				
	φ_{CNT} (%)					φ_{CNT} (%)				
	0.1	0.3	0.5	0.7	0.9	0.1	0.3	0.5	0.7	0.9
$\mu_{nf} \times 10^4$ (kg/ms)	8.15	9.48	11.08	12.81	14.48	11.33	13.03	14.61	15.95	17.01
k_{nf} (W/mK)	0.691	0.725	0.739	0.759	0.794	0.703	0.759	0.772	0.866	0.902

135

136   Moreover, the nanofluid bulk density (ρ_{nf}) and specific heat ($c_{p,nf}$) are computed as:

$$\rho_{nf} = \varphi_M \rho_M + \varphi_{CNT} \rho_{CNT} + (1 - \varphi_M - \varphi_{CNT})\rho_w \tag{1}$$

$$c_{p,nf} = \varphi_M c_{p,M} + \varphi_{CNT} c_{p,CNT} + (1 - \varphi_M - \varphi_{CNT})c_{p,w} \tag{2}$$

137   where φ is the volume concentration of nanoparticles and, subscripts *M, CNT* and *w* refer to

138   magnetite, CNT and water, respectively.

139

140   **3. Mathematical modelling**

141   Due to the small size of nanofluids, they can thus be approximately evaluated as a pure fluid

142   considering no velocity slip and local thermal equilibrium between the base fluid and

143   nanoparticles. The governing equations for laminar, steady state forced convection flow of the

144   studied nanofluid are given as follows:

145   Continuity:

$$\nabla \cdot \left(\rho_{nf} V \right) = 0 \tag{3}$$

146 Momentum:

$$\nabla \cdot \left(\rho_{nf} VV \right) = -\nabla p + \nabla \cdot \left(\mu_{nf} \nabla V \right) \tag{4}$$

147 Energy:

$$\nabla \cdot \left(\rho V c_{p,nf} T \right) = \nabla \cdot \left(k_{nf} \nabla T \right) \tag{5}$$

148 where V is the velocity, p is the pressure, and T is the temperature.

149 Reynolds number for the flow of nanofluid (Re_{nf}) and water (Re_w) through the tube side and

150 annulus side, respectively, can be calculated as:

$$Re_{nf} = \frac{\rho_{nf} u_{in,nf} (2r_i)}{\mu_{nf}} \tag{6}$$

$$Re_w = \frac{\rho_w u_{in,w} [2(r_o - r_i)]}{\mu_w} \tag{7}$$

151 where $u_{in,nf}$ and $u_{in,w}$ are the inlet velocity of the nanofluid and water, respectively.

152 Considering the fact that the outer wall of the heat exchanger is adiabatic and the problem under

153 consideration is steady state, the rate of heat transfer to the nanofluid from the hot water is equal

154 to that of the hot water according to the conservation of energy $(\dot{Q}_{nf} = \dot{Q}_w = \dot{Q})$ which are

155 obtained as:

$$\dot{Q}_{nf} = \dot{m}_{nf} c_{p,nf} (T_{out} - T_{in})_{nf} \tag{8}$$

$$\dot{Q}_w = \dot{m}_w c_{p,w} (T_{in} - T_{out})_w \tag{9}$$

156 where $\dot{m}_{nf}$ and $\dot{m}_w$ are mass flow rate of the cold nanofluid and the hot water, respectively.

157 The overall heat transfer coefficient is given as:

$$U = \frac{\dot{Q}}{A \Delta T_{LMTD}} \tag{10}$$

9

158 where A is the internal tube area, and ΔT_{LMTD} is the logarithmic mean temperature difference

159 computed as:

$$\Delta T_{LMTD} = \frac{\Delta T_2 - \Delta T_1}{\ln(\Delta T_2/\Delta T_1)} \tag{11}$$

160 where $\Delta T_1 = T_{in,w} - T_{out,nf}$ and $\Delta T_2 = T_{out,w} - T_{in,nf}$.

161 One way of measuring the performance of a heat exchanger is to compute its effectiveness. The

162 heat exchanger effectiveness is ratio of the actual heat transfer rate to the maximum possible one

163 given as:

$$\varepsilon = \frac{\dot{Q}}{\dot{Q}_{max}} = \frac{\dot{Q}}{C_{min}(T_{in,w} - T_{in,nf})} \tag{12}$$

164 where C_{min} represents the minimum heat capacity rate given as:

$$C_{min} = \min[C_w, C_{nf}] \tag{13}$$

165 Here, C_w and C_{nf} are respectively heat capacity rates of the water and the nanofluid defined as:

$$C_w = \dot{m}_w c_{p,w} \tag{14}$$

$$C_{nf} = \dot{m}_{nf} c_{p,nf} \tag{15}$$

166 The minimum heat capacity rate is obtained for the nanofluid and hence, the effectiveness is

167 calculated as:

$$\varepsilon = \frac{T_{out,nf} - T_{in,nf}}{T_{in,w} - T_{in,nf}} \tag{16}$$

168 The rate of energy consumption required to pump the nanofluid in the heat exchanger is given as:

$$\dot{W} = \dot{V}\Delta p \tag{17}$$

169 where $\dot{V}$ and Δp denote volumetric flow rate and pressure drop, respectively.

170 To evaluate the heat transfer rate and the pumping power simultaneously, a parameter called

171 performance index is defined as the ratio of heat transfer rate to the pressure drop given as [52]:

10

$$\eta = \frac{\dot{Q}}{\Delta p} \tag{18}$$

172

4. Numerical method and validation

174   ANSYS-FLUENT software is used to solve the governing equations employing the SIMPLE

175   method for pressure and velocity coupling. The second order upwind method is used to discretize

176   the convective and diffusion terms using the finite-volume method. The convergence criteria is

177   also set to 10^{-6}. A structured quad based mesh was used throughout the domain with a more grid

178   density near the wall. The grid independence study was carried out by considering the numerical

179   results of six different grid resolutions. The results of this investigation is summarized in Table 2.

180   It should be noted that the grid resolution was reported as number of longitudinal nodes×number

181   of radial nodes in central tube×number of radial nodes in annulus. So, by comparing the results,

182   the grid with resolution of 1000×35×35 was chosen. To verify the present numerical procedure,

183   the results are compared with the experimental data of Duangthongsuk and Wongwises [53] for

184   water-TiO_2 nanofluid in a double-pipe heat exchanger shown in Fig. 2. Good agreement between

185   the present results and Ref. [53] is shown with the maximum error of about 5%.

186

187   **Table 2.** Grid independence study for non-Newtonian Fe_3O_4-CNT/water hybrid nanofluid at $\varphi_M = 0.9\%$, $\varphi_{CNT} =$

188   1.35% and $Re = 2000$.

Grid	$\dot{Q}$ (W)	Percentage difference	ΔP(Pa)	Percentage difference
800×25×25	33.92		120.1	
900×30×30	35.82	5.6	125.5	4.5
950×30×30	37.06	3.5	129.1	2.9

11

|				
1000×30×30	37.92	2.3	132.1	2.3
1000×35×35	**38.23**	**0.8**	**133.7**	**1.2**
1100×35×35	38.51	0.7	134.6	0.67

189
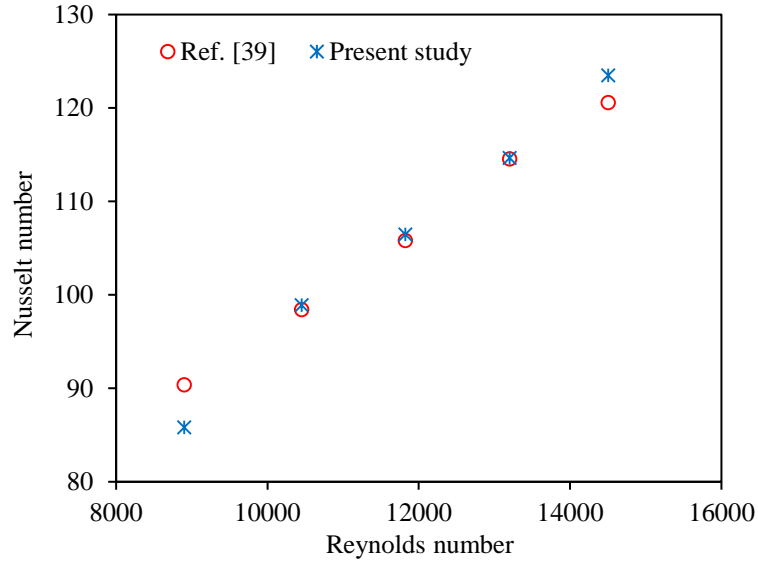
Fig. 2. Comparison between results obtained from present study and experimental results of Ref. [53].

190

5. Geometry and boundary conditions

The present investigation is conducted in a double-pipe counter-current mini-channel heat exchanger with the length of 1 m, inner diameter of 1 mm, and outer diameter of 2 mm. The thickness of the inner tube's wall is neglected. Fig. 3 illustrates the schematic of the geometry including the flow directions of both hot water and cold nanofluid. Due to the axisymmetric nature of the problem, only half of the geometry is considered as the computational 2-D domain. For the outer wall, adiabatic boundary condition is used. Uniform velocity and uniform temperature are

198 also considered at both tube and annulus entrances while zero relative pressure is utilized at the

199 outlets. Additionally, the no-slip condition is employed on the inner and outer walls.

200
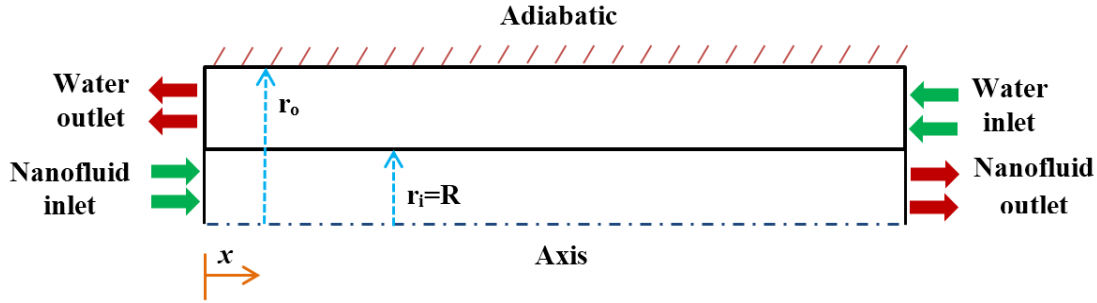

Fig. 3. The mini-channel heat exchanger under study.

201

202 **6. Results and discussion**

203 In this research, the influences of the shear rate and temperature dependent viscosity and the

204 temperature-dependent thermal conductivity on the hydrothermal characteristics of Fe_3O_4-

205 CNT/water hybrid nanofluid flowing inside a double-pipe heat exchanger are evaluated and

206 compared with those obtained by regarding the hybrid nanofluid as a Newtonian fluid with

207 constant thermal conductivity and viscosity. The simulations are conducted at magnetite

208 concentration range of 0.1-0.9%, CNT concentration range of 0-1.35%, Reynolds number range

209 of 500-2000 for the tube side, and constant Reynolds number of 1000 for the annulus side. The

210 inlet temperature of the nanofluid and water are considered as 298 K and 308 K, respectively. Note

211 that the results of the non-Newtonian and Newtonian Fe_3O_4-CNT/water hybrid nanofluids will be

212 reported by letters 'NN' and 'N', respectively.

213 Fig. 4 illustrates the variations of viscosity ratio $(\mu_{nf,NN}/\mu_{nf,N})$ for $\varphi_M = 0.7\%$ and $\varphi_{CNT} = 0.7\%$

214 at three different cross sections (i.e. $x=0.1$ m, $x=0.5$ m, and $x=0.9$ m). For $Re = 500$, by

215 increasing the distance from the tube axis, viscosity of the non-Newtonian hybrid nanofluid

13

216   diminishes severely at first, and then its descending trend continues at a milder slope, and degree

217   of variations increases with increase in distance from the tube inlet. Near the tube axis, due to

218   small values of shear rate and temperature, viscosity is high. However, by moving away from the

219   tube axis toward the tube wall, both shear rate and temperature increase and consequently,

220   viscosity reduces. The results for $Re = 2000$ indicate that by moving away from the central

221   regions of tube toward the tube wall, viscosity reduces and degree of viscosity variation is lower

222   than that for $Re = 500$. By increasing the Reynolds number at a fixed concentration, the thickness

223   of velocity boundary layer reduces and therefore, the velocity gradient increases. Therefore, there

224   are two reasons for the negligible changes of viscosity in central regions of tube at cross-section

225    $x=0.1$ m. The first reason is that the shear rate is greater than 60 s^{-1} at most of points of this section,

226   and consequently, fluid viscosity is constant. The second reason is that the thickness of thermal

227   boundary layer in this area is small, which causes constant temperature of the hybrid nanofluid in

228   central regions of tube and thus, viscosity remains unchanged. By moving away from the tube

229   inlet, the thermal boundary layer grows which raises the temperature of the nanofluid in vicinity

230   of the tube wall and, thus, reduces the viscosity. Therefore, the velocity of nanofluid diminishes

231   near the tube wall and increases at the tube axis; i.e. the velocity profile becomes flatter. As a

232   result, the amount of shear rate increases near the tube wall and diminishes near the tube axis;

233   which causes viscosity to diminish near the tube wall and increase near the tube axis. Therefore, it

234   can be said that by moving away from the tube axis, viscosity of the non-Newtonian hybrid

235   nanofluid near the tube wall diminishes; however, its behavior near the tube axis depends on

236   whether the effect of viscosity decrease due to the rise of temperature is greater or the effect of

237   viscosity increase due to the reduction of velocity gradient. Therefore, it is concluded that the

238   effect of temperature increase overcomes the effect of temperature gradient reduction, and

14

239   viscosity of the non-Newtonian nanofluid diminishes by moving away from the tube inlet.

240   Furthermore, Figs. 4(a) and 4(b) show that viscosity of the non-Newtonian nanofluid diminishes

241   with the increase of Reynolds number. This can be justified based on the reduction of the velocity

242   boundary layer thickness with increasing the Reynolds number, which leads to the increase of

243   velocity gradient and thus the reduction of fluid viscosity. In addition, the comparison between the

244   viscosities of the Newtonian and non-Newtonian hybrid nanofluids indicates that in central regions

245   of the tube, viscosity of the non-Newtonian nanofluid is greater than that of the Newtonian

246   nanofluid; however, in vicinity of the tube wall, the Newtonian fluid has a higher viscosity and by

247   moving away from the tube inlet, the region in which viscosity of the Newtonian nanofluid is

248   greater becomes vaster, since the viscosity of the non-Newtonian nanofluid diminishes by moving

249   away from the tube wall. Both the temperature and shear rate are higher near the tube wall than

250   the tube axis. Therefore, both of these factors lead to the viscosity reduction of the non-Newtonian

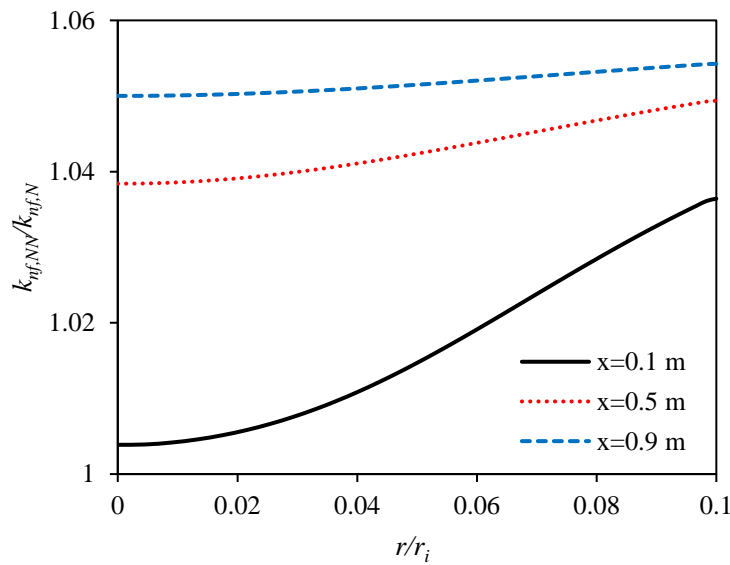251   nanofluids, while the opposite is true near the tube axis.

252
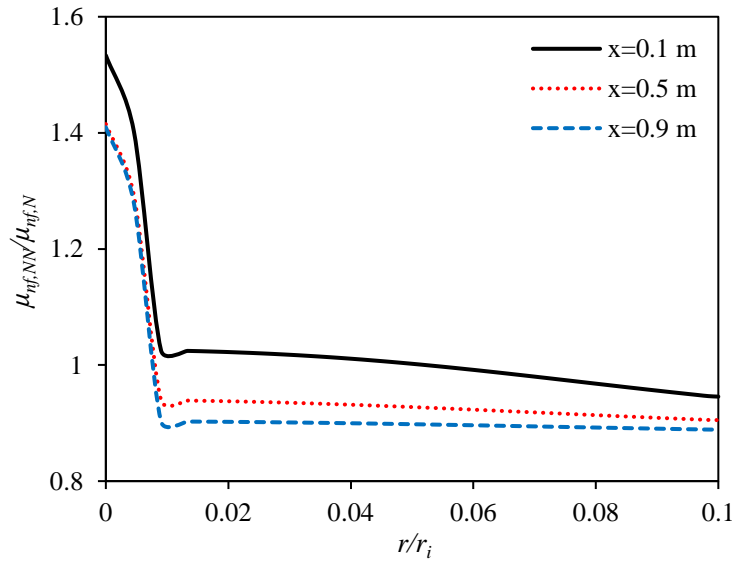
(a)
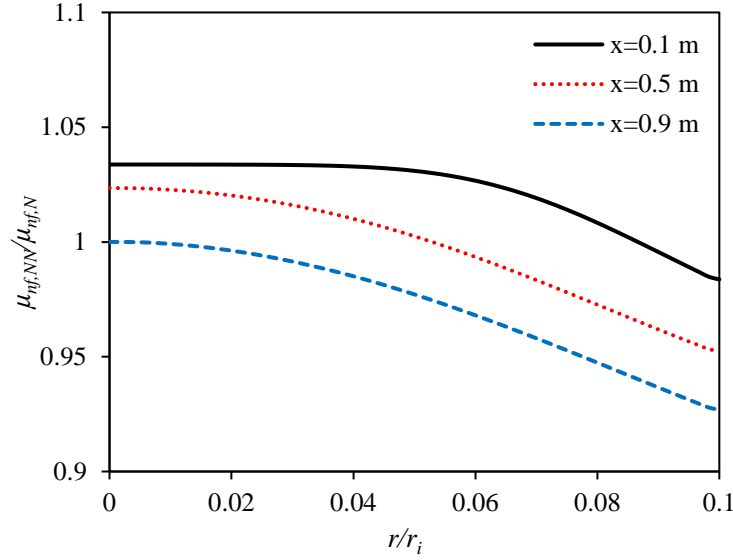
(b)

Fig. 4. Viscosity ratio for $\varphi_M = 0.7\%$ and $\varphi_{CNT} = 0.7\%$ at three different cross sections for (a) $Re = 500$ and
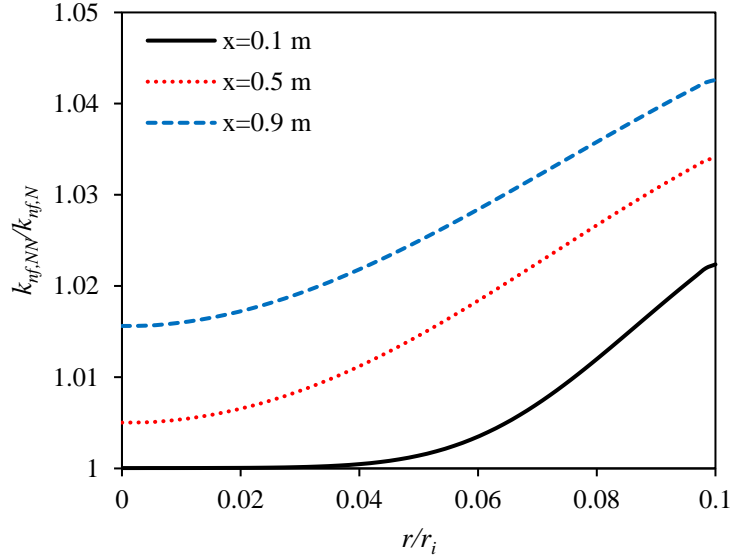
(b) $Re = 2000$.

253

254   Fig. 5 displays the variations of thermal conductivity ratio $(k_{nf,NN}/k_{nf,N})$ for $\varphi_M = 0.7\%$ and

255    $\varphi_{CNT} = 0.7\%$ at three different cross sections (i.e. x=0.1 m, x=0.5 m, and x=0.9 m). For $Re =$

256   500, by moving away from the tube axis toward the tube wall, thermal conductivity of the non-

257   Newtonian nanofluid increases continually due to the higher temperature of nanofluid near the

258   wall. The improvement of thermal conductivity with the increase of distance from the tube inlet is

259   due to the higher nanofluid temperature resulting from the increase of heat transfer to the nanofluid.

260   Similar observations exist for $Re = 2000$, with the difference that the slope of thermal

261   conductivity increment near the tube wall is greater for $Re = 2000$. This is due to the rise of

262   nanofluid temperature near the tube wall, resulting from the lower thermal boundary layer

263   thickness that occurs because of the flow velocity enhancement. Moreover, the comparison

264   between thermal conductivity of the Newtonian and non-Newtonian nanofluids shows that thermal

16

265   conductivity of the non-Newtonian nanofluid is always greater than that of the Newtonian

266   nanofluid; however, the difference between thermal conductivities of the nanofluids reduces with

267   the increase of Reynolds number. Considering the fact that the inlet temperature of nanofluid is 25

268   ºC, and the thermal conductivity improves with the rise of temperature, it was predictable for the

269   thermal conductivity of non-Newtonian nanofluid to always surpass that for the Newtonian

270   nanofluid. In addition, increasing the Reynolds number reduces the thermal boundary layer

271   thickness and consequently, the internal layers of nanofluid are affected more slowly by wall

272   temperature. This reduces the nanofluid temperature and thereby reduces the thermal conductivity

273   of non-Newtonian nanofluid.

274

(a)

(b)

Fig. 5. Thermal conductivity ratio for $\varphi_M = 0.7\%$ and $\varphi_{CNT} = 0.7\%$ at three different cross sections for (a) $Re = 500$ and (b) $Re = 2000$.

275

276   Fig. 6 demonstrates the difference between the pressure drop of the Newtonian and non-Newtonian

277   Fe$_3$O$_4$-CNT/water hybrid nanofluids $\left(d_{\Delta p} = \frac{(\Delta p)_{NN} - (\Delta p)_N}{(\Delta p)_N} \times 100\right)$ in terms of magnetite

278   concentration at different Reynolds numbers. It is seen that the pressure drop of the non-Newtonian

279   nanofluid is always less than that of the Newtonian nanofluid. The minimum pressure drop

280   difference (1.5%) is obtained at $\varphi_M = 0.9\%$, $\varphi_{CNT} = 1.35\%$ and $Re = 2000$, while the maximum

281   difference (9.71%) occurs at $\varphi_M = 0.5\%$, $\varphi_{CNT} = 0.1\%$ and $Re = 500$. Additionally, it is

282   observed that the difference between the pressure drop of the Newtonian and non-Newtonian

283   nanofluids reduces with the increase of Reynolds number. According to Fig. 4, this is caused by

284   the reduction in the difference between the average viscosity of the Newtonian and non-Newtonian

285   nanofluids by increasing the Reynolds number. Furthermore, at $\varphi_{CNT} = 0.1\%$, the pressure drop

286   difference augments when the magnetite concentration increases from 0.1 to 0.3% and then

18

287   reduces by the further increment of magnetite concentration; while for $\varphi_{CNT} = 1.35\%$, the

288   increase of magnetite concentration results in the reduction in the pressure drop difference.

289   Besides, at $\varphi_M = 0.1\%$, the pressure drop difference rises with increasing the CNT concentration

290   from 0.1 to 1.35%, while the opposite is true at higher magnetite concentrations. According to

291   Darcy's equation ($\Delta p = f \frac{L}{2r_i} \frac{\rho u_{in}^2}{2}$, where f is the friction factor defined as $f = \frac{64}{Re}$ [54]) and by

292   considering the fact that the non-Newtonian and Newtonian nanofluids have the same density and

293   friction factor at an identical Reynolds number, the difference between the pressure drop of the

294   Newtonian and non-Newtonian nanofluids is only due to the difference between their viscosities.

295   It can be concluded from the presented results that the assumption of constant thermal conductivity

296   and viscosity of the hybrid nanofluid, at a low Reynolds number, leads to large errors in the

297   computation of pressure drop; however, the obtained error decreases with the increase of Reynolds

298   number.

299
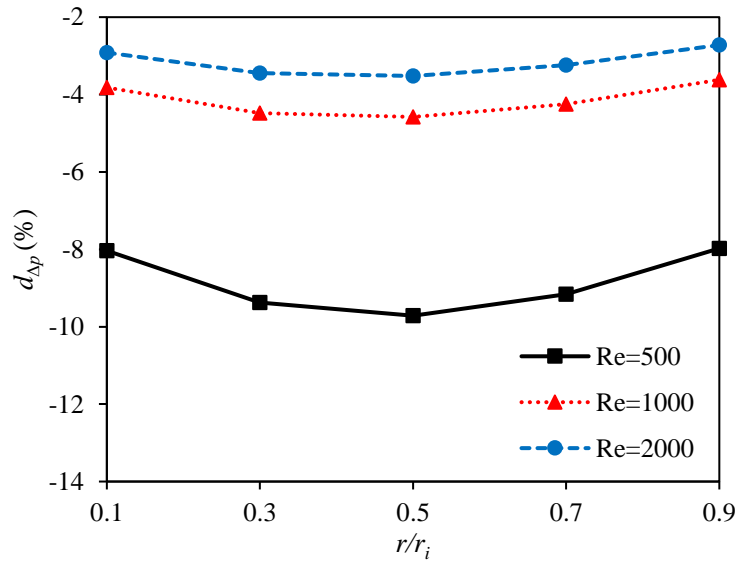
(a)
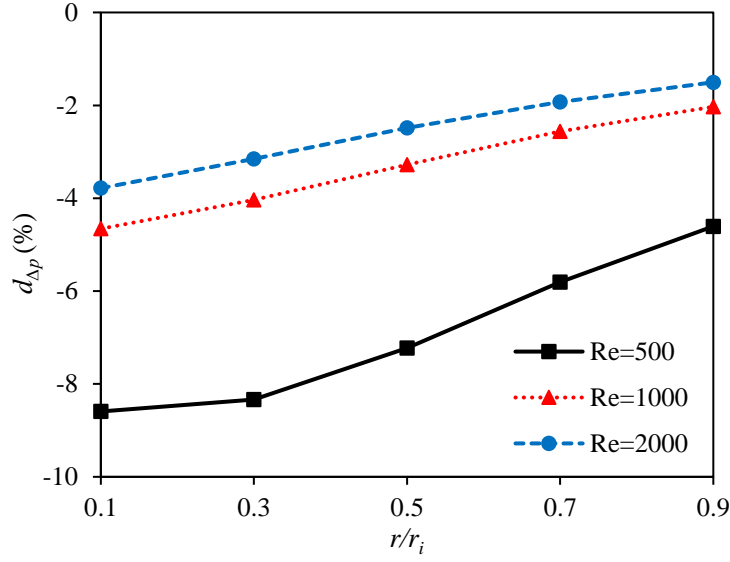
(b)

Fig. 6. Pressure drop at different Reynolds numbers in terms of magnetite concentration at (a) $\varphi_{CNT} = 0.1\%$ and

(b) $\varphi_{CNT} = 1.35\%$.

300

301   The effects of magnetite concentration on the difference between the heat transfer rate of the

302   Newtonian and non-Newtonian Fe₃O₄-CNT/water hybrid nanofluids ($d_Q = \frac{\dot{Q}_{NN} - \dot{Q}_N}{\dot{Q}_N} \times 100$) at

303   different Reynolds numbers are illustrated in Fig. 7. It is seen that the heat transfer rate of the non-

304   Newtonian hybrid nanofluid is greater than that of the Newtonian nanofluid. The minimum

305   difference (0.31%) is achieved at $\varphi_M = 0.9\%$, $\varphi_{CNT} = 1.35\%$ and $Re = 500$, while the maximum

306   difference (1.23%) occurs at $\varphi_M = 0.1\%$, $\varphi_{CNT} = 1.35\%$ and $Re = 1000$. Additionally, it is

307   observed that with increase in the Reynolds number, the difference between the heat transfer rate

308   of the non-Newtonian and Newtonian nanofluids increases first and then decreases. Increasing the

309   Reynolds number reduces the thermal conductivity and the thermal boundary layer thickness of

310   the non-Newtonian nanofluid, which respectively reduces and increases the rate of heat transfer.

311   In view of Fig. 7, it can be realized that at $Re = 1000$, the effect of reducing the thickness of

20

312   thermal boundary layer is dominant in comparison with the reduction of thermal conductivity and

313   therefore, the difference between the heat transfer rate of the Newtonian and non-Newtonian

314   nanofluids increases. Meanwhile, for $Re = 2000$, the reduction of thermal conductivity is

315   dominant, which causes a decrease in the difference between the heat transfer rate of the non-

316   Newtonian and Newtonian nanofluids. Moreover, Fig. 7 reveals that at magnetite concentrations

317   of 0.1% and 0.3%, increasing the CNT concentration form 0.1% to 1.35% leads to an increase in

318   the difference between the heat transfer rate of the Newtonian and non-Newtonian nanofluids,

319   whereas the opposite is true for higher magnetite concentrations. Increasing the magnetite

320   concentration leads to the increase of thermal conductivity of the non-Newtonian nanofluid and

321   therefore, the increase of nanofluid outlet temperature, and eventually to the increase of difference

322   between the heat transfer rate of the non-Newtonian and Newtonian nanofluids. Further increase

323   in the magnetite concentration leads to the decrease of the difference between the thermal

324   conductivity of the non-Newtonian and Newtonian nanofluids and therefore, the decrease of the

325   heat transfer rate difference. The results also show that there is no specific pattern on the

326   relationship between the difference in the heat transfer rate of the Newtonian and non-Newtonian

327   nanofluids and the magnetite concentration.
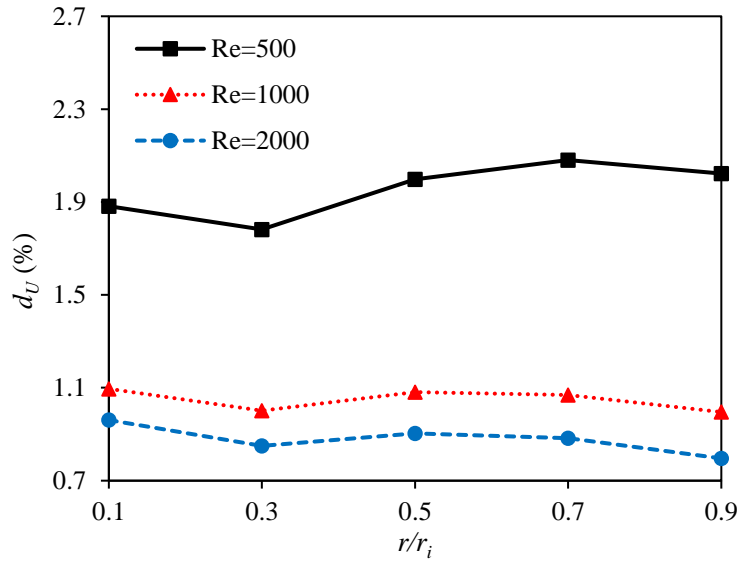
328
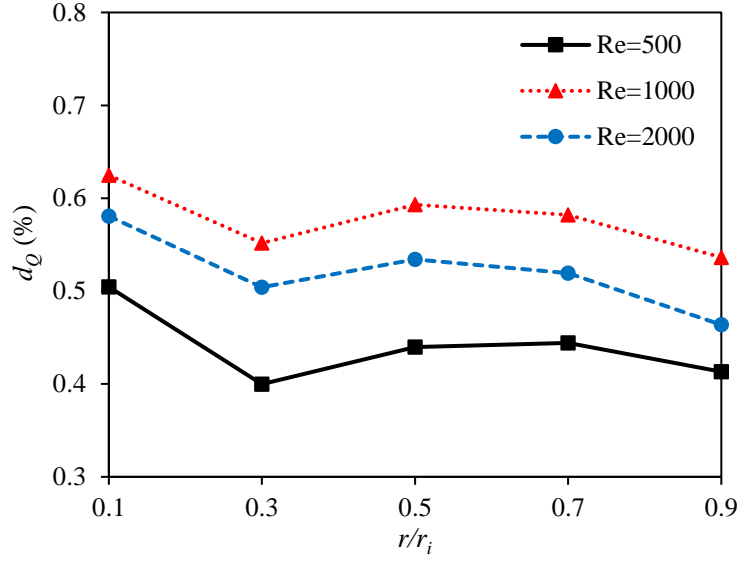
(a)
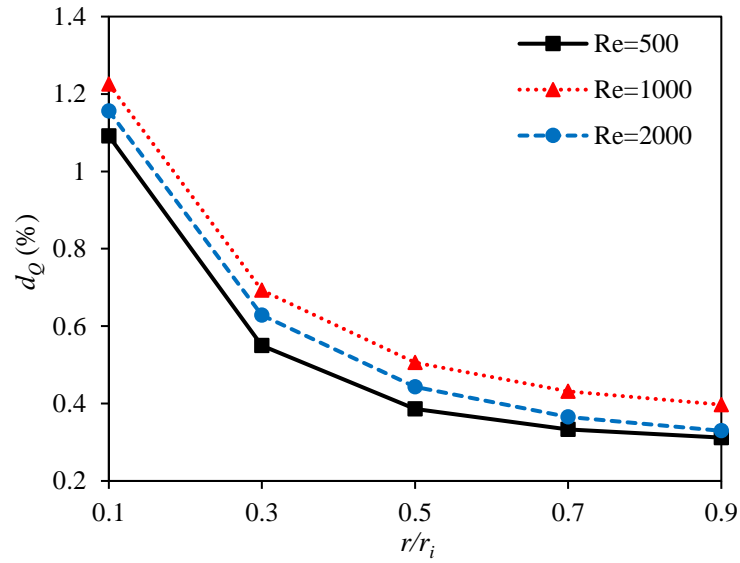
(b)

Fig. 7. Heat transfer rate at different Reynolds numbers in terms of magnetite concentration at (a) $\varphi_{CNT} = 0.1\%$

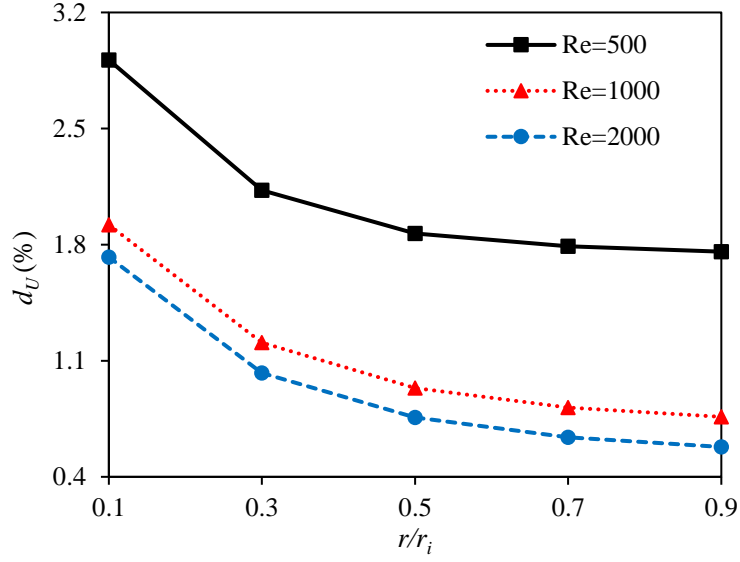and (b) $\varphi_{CNT} = 1.35\%$.

329

330   Fig. 8 shows the difference between the overall heat transfer coefficient of the Newtonian and non-

331   Newtonian Fe_3O_4-CNT/water hybrid nanofluids ($d_U = \frac{U_{NN}-U_N}{U_N} \times 100$) in terms of magnetite

332 concentration at various Reynolds numbers. It is clear that the overall heat transfer coefficient of

333 the non-Newtonian hybrid nanofluid is greater than that of the Newtonian nanofluid. The minimum

334 difference of the overall heat transfer coefficients (0.58%) is obtained at $\varphi_M = 0.9\%$, $\varphi_{CNT} =$

335 1.35% and $Re = 2000$, while the maximum difference (2.91%) is achieved at $\varphi_M = 0.1\%$,

336 $\varphi_{CNT} = 1.35\%$ and $Re = 500$. Furthermore, the results depicted that the variations of difference

337 between the overall heat transfer coefficient of the Newtonian and non-Newtonian nanofluids with

338 the magnetite and CNT concentrations are similar to that of the difference between the heat transfer

339 rate of these nanofluids. According to the results presented in Fig. 8, it can be concluded that the

340 difference between the overall heat transfer coefficienct of the Newtonian and non-Newtonian

341 nanofluids is less than 3%, which is not significant.

342

(a)

(b)

Fig. 8. Overall heat transfer coefficient at different Reynolds numbers in terms of magnetite concentration at (a) $\varphi_{CNT} = 0.1\%$ and (b) $\varphi_{CNT} = 1.35\%$.

343

344   The impacts of magnetite concentration on the difference between the effectiveness of the heat

345   exchangers containing Newtonian and non-Newtonian Fe_3O_4-CNT/water hybrid nanofluids ($d_\varepsilon =$

346    $\frac{\varepsilon_{NN}-\varepsilon_N}{\varepsilon_N} \times 100$) at different Reynolds numbers are illustrated in Fig. 9. In view of Eq. (12), it can
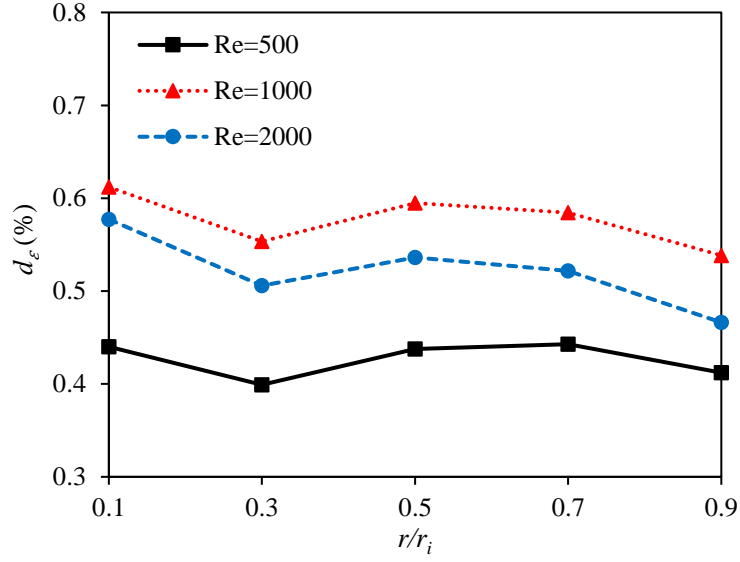
347   be realized that the trend of effectiveness variations is similar to that of the heat transfer rate

348   variations. Therefore, all the conclusions reached above regarding the heat transfer rate are also
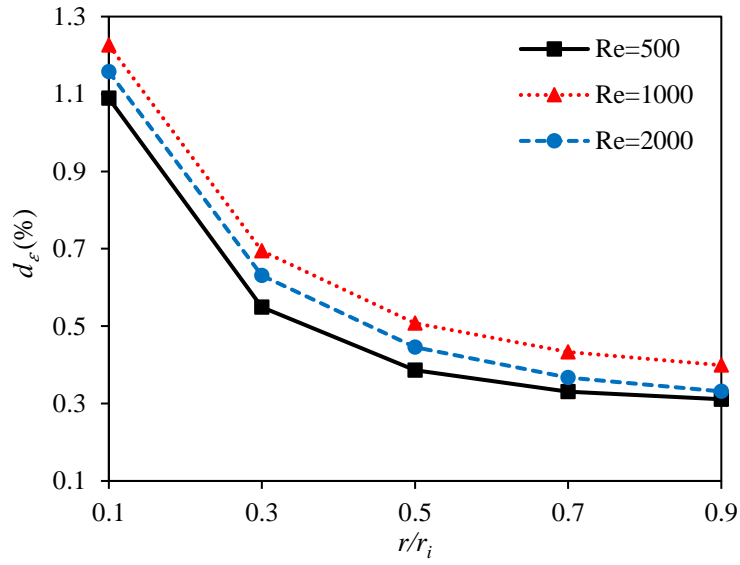
349   true for the effectiveness.

350

(a)

(b)

Fig. 9. Effectiveness of heat exchanger at different Reynolds numbers in terms of magnetite concentration at (a)
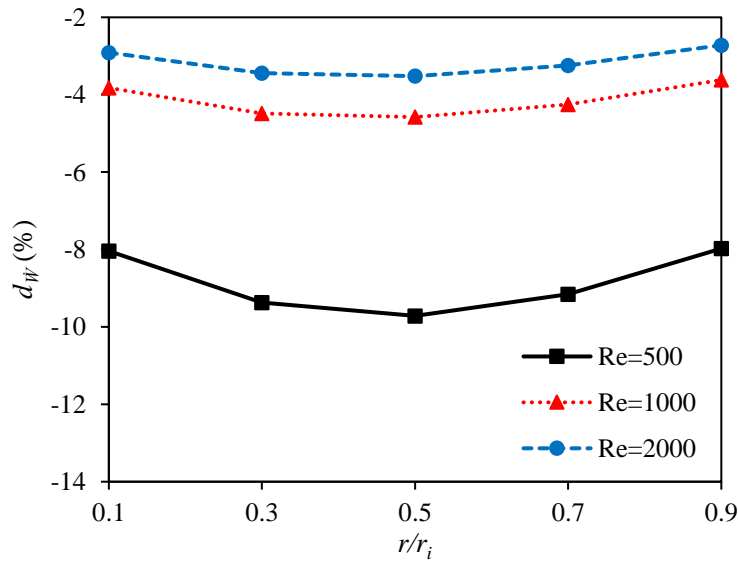
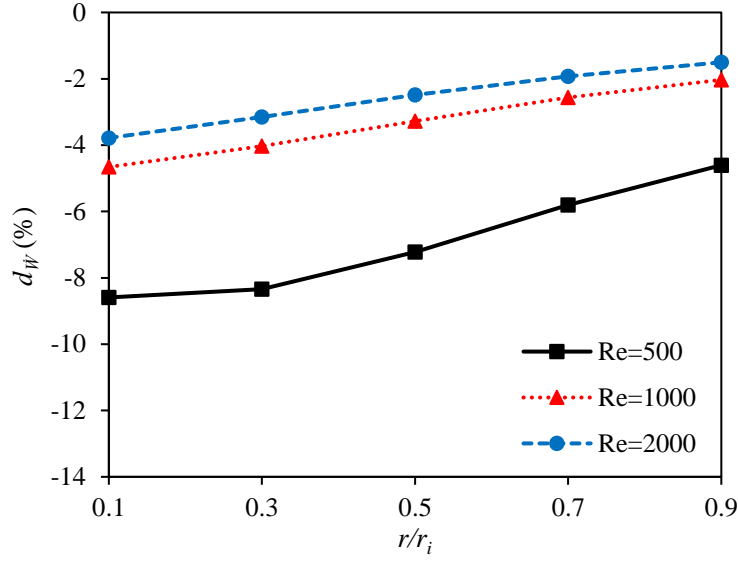$\varphi_{CNT} = 0.1\%$ and (b) $\varphi_{CNT} = 1.35\%$.

351

352   The pumping power indicates the amount of energy utilized in a heat exchanger. Fig. 10 depicts

353   the difference between the pumping powers of the Newtonian and non-Newtonian Fe_3O_4-

354 CNT/water hybrid nanofluids ($d_U = \frac{U_{NN}-U_N}{U_N} \times 100$) in terms of magnetite concentration at

355 different Reynolds numbers. It is seen that at a constant Reynolds number, the non-Newtonian

356 hybrid nanofluid always requires less pumping power than the Newtonian nanofluid. The

357 minimum pumping power difference (1.5%) is obtained at $\varphi_M = 0.9\%$, $\varphi_{CNT} = 1.35\%$ and $Re =$

358 2000, while the maximum difference (9.71%) occurs at $\varphi_M = 0.5\%$, $\varphi_{CNT} = 0.1\%$ and $Re =$

359 500. In view of Eq. (17), and considering the same average velocity for Newtonian and non-

360 Newtonian nanofluids at similar Reynolds numbers, the difference between the pumping power of

361 the Newtonian and non-Newtonian nanofluids is only related to the difference between their

362 pressure drops. Therefore, at a low Reynolds number, the assumption of constant properties leads

363 to a considerable increase in the pumping power of heat exchangers, whereas the difference

364 reduces with increasing the Reynolds number.

365

(a)

(b)

Fig. 10. Pumping power of heat exchanger at different Reynolds numbers in terms of magnetite concentration at

(a) $\varphi_{CNT} = 0.1\%$ and (b) $\varphi_{CNT} = 1.35\%$.

366

367 The influences of magnetite concentration on the difference between the performance index of the

368 heat exchangers containing Newtonian and non-Newtonian Fe_3O_4-CNT/water hybrid nanofluids

369 ($d_\varepsilon = \frac{\eta_{NN} - \eta_N}{\eta_N} \times 100$) at different Reynolds numbers are displayed in Fig. 11. It is observed that

370 the heat exchanger containing non-Newtonian nanofluid has a higher performance index than that

371 containing Newtonian nanofluid. The minimum difference (1.86%) is obtained at $\varphi_M = 0.9\%$,

372 $\varphi_{CNT} = 1.35\%$ and $Re = 2000$, while the maximum difference (11.25%) is achieved at $\varphi_M =$

373 0.5%, $\varphi_{CNT} = 0.1\%$ and $Re = 500$. Moreover, it is seen that the difference between the

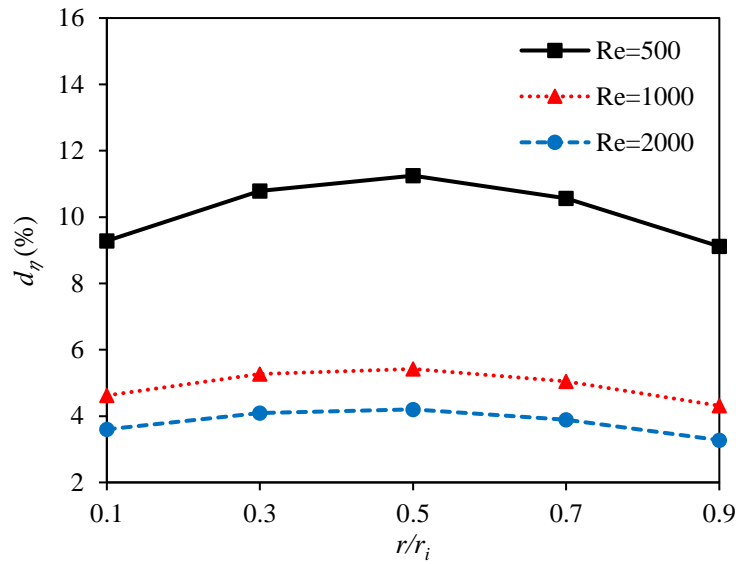374 performance index of the heat exchangers containing Newtonian and non-Newtonian nanofluids

375 reduces with increase in the Reynolds number. In addition, at $\varphi_{CNT} = 0.1\%$, the performance

376 index difference augments when the magnetite concentration rises from 0.1 to 0.5% and then

377 decreases by the further increment of magnetite concentration; while for $\varphi_{CNT} = 1.35\%$, the

27

378 increase of magnetite concentration results in the reduction in the performance index difference.

379 Moreover, at $\varphi_M = 0.1\%$, the performance index difference increases with increase in CNT

380 concentration from 0.1 to 1.35%, while the opposite is happen at higher magnetite concentrations.

381 Finally, it can be said that the assumption of constant properties of the Fe_3O_4-CNT/water hybrid

382 nanofluid at low Reynolds numbers and high concentrations of magnetite and CNT nanoparticles,

383 leads to large errors in the computation of performance index of heat exchanger.

384

(a)
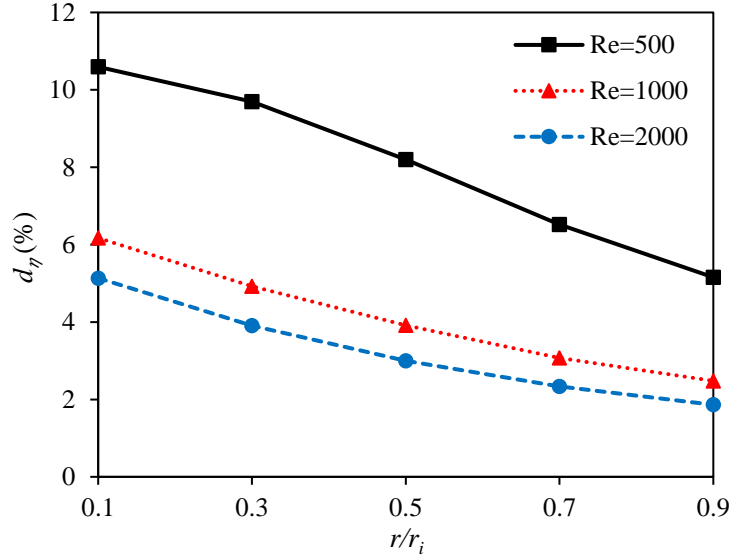
Fig. 11. Performance index of heat exchanger at different Reynolds numbers in terms of magnetite concentration

at (a) $\varphi_{CNT} = 0.1\%$ and (b) $\varphi_{CNT} = 1.35\%$.

385

386   **7. Conclusion**

387   In this research, the hydrothermal performance of the non-Newtonian Fe_3O_4-CNT/water hybrid

388   nanofluid considering temperature-dependent thermal conductivity and viscosity is numerically

389   evaluated in a double-pipe mini-channel heat exchanger compared with Newtonian Fe_3O_4-

390   CNT/water nanofluid with constant thermal conductivity and viscosity. The comparison is used in

391   order to find how the assumption of constant thermophysical properties of a hybrid nanofluid

392   affects the hydrothermal characteristics in a double-pipe heat exchanger. The obtained results show

393   that in central region of the tube, the non-Newtonian hybrid nanofluid has a higher viscosity

394   compared to the Newtonian nanofluid, while the opposite is true in vicinity of the tube wall.

395   Besides, it is found that the non-Newtonian hybrid nanofluid always has a higher thermal

396   conductivity than the Newtonian nanofluid. In addition, it is seen that the heat transfer rate, overall

29

397   heat transfer coefficient, effectiveness, and performance index of the non-Newtonian hybrid

398   nanofluid are greater than those of the Newtonian hybrid nanofluid, while the opposite is true for

399   pressure drop and pumping power. The difference between heat transfer rate, overall heat transfer

400   coefficient, effectiveness, and performance index of Newtonian and non-Newtonian hybrid

401   nanofluids augments with increase in the Reynolds number, whereas the difference between the

402   pressure drop and pumping power of nanofluids reduces with increasing the Reynolds number.

403   Furthermore, increment in magnetite and CNT concentrations has no particular effect on the

404   considered parameters. Finally, it can be concluded that by supposing that the Fe_3O_4-CNT/water

405   hybrid nanofluid is a Newtonian fluid with constant thermal conductivity and viscosity, large

406   errors occur in the computation of pressure drop, pumping power, and performance index, whereas

407   the errors in the computation of heat transfer rate, overall heat transfer coefficient, and

408   effectiveness aren't considerable. The results of this study could provide guidelines to better

409   understand the real behaviors of hybrid nanofluids in heat exchangers.

410

411   **Appendix A**

412   The thermal conductivity correlation:

413     $k_{nf} = 0.22274 \tanh(-0.02119T + 0.09807\varphi_M - 0.06975\varphi_{CNT} + 0.02528) - 0.67299 \tanh(-0.00379T$

414     $- 0.69125\varphi_M + 0.11290\varphi_{CNT} + 0.03221) - 0.26968 \tanh(0.12778T + 0.00334\varphi_M - 0.00362\varphi_{CNT} +$

415     $0.00284) - 0.22184 \tanh(0.02121T - 0.09748\varphi_M + 0.06875\varphi_{CNT} - 0.02471) - 1.01112 \tanh$

416     $(0.00755T - 0.99285\varphi_M - 0.05887\varphi_{CNT} - 0.42417) - 1.04948 \tanh(-0.00513T + 0.10775\varphi_M -$

417     $1.43226\varphi_{CNT} - 0.49474) + 0.51061 \tanh(0.00157T - 1.10296\varphi_M - 1.32512\varphi_{CNT} + 0.43476) +$

418     $0.23038 \tanh(-0.02104T + 0.10309\varphi_M - 0.07821\varphi_{CNT} + 0.03035) + 0.08974 \tanh(0.00333T +$

419     $0.05961\varphi_M + 0.02413\varphi_{CNT} - 0.03048) + 0.45090 \tanh(0.02304T - 0.13733\varphi_M - 0.48067\varphi_{CNT} -$

$0.50330) - 0.36153 \tanh (-0.06346T + 0.10622\varphi_M + 0.33903\varphi_{CNT} + 0.29052) - 0.49423 \tanh (-$

$0.00131T + 1.70368\varphi_M - 0.87848\varphi_{CNT} - 0.19465) - 0.21662 \tanh (0.02131T - 0.09401\varphi_M +$

$0.06297\varphi_{CNT} - 0.02155) - 0.57108 \tanh (-0.00374T - 0.59628\varphi_M + 0.10685\varphi_{CNT} + 0.04961) -$

$$0.27492 \tag{A.1}$$

The viscosity correlation:

$\mu_{nf} = -0.24861 \tanh (0.04611\gamma - 0.00068T + 1.06226\varphi_M + 0.13756\varphi_{CNT} + 1.43142) + 1.03130$

$\tanh (0.47273\gamma + 0.00143T - 0.04534\varphi_M - 0.02812\varphi_{CNT} + 0.40817) - 0.20231 \tanh (-0.17180\gamma +$

$0.00067T + 1.20978\varphi_M - 0.18044\varphi_{CNT} - 0.25325) - 0.32811 \tanh (0.13316\gamma - 0.00050T -$

$1.21402\varphi_M + 0.14462\varphi_{CNT} + 0.53138) + 0.30415 \tanh (-0.11840\gamma - 0.00165T + 4.60293\varphi_M -$

$0.72515\varphi_{CNT} - 3.12857) - 0.00215 \tanh (-0.31607\gamma + 0.00027T - 0.98832\varphi_M + 0.15752\varphi_{CNT} +$

$4.97709) + 0.41053 \tanh (0.11589\gamma + 0.00148T - 4.37455\varphi_M + 0.62623\varphi_{CNT} + 3.03569) + 0.04707$

$\tanh (-0.09258\gamma - 0.04017T + 1.06859\varphi_M - 0.09049\varphi_{CNT} - 0.48490) + 0.59719 \tanh (0.04287\gamma +$

$0.33517T + 1.13670\varphi_M - 0.95007\varphi_{CNT} + 0.04857) + 0.03178 \tanh (-0.02358\gamma - 0.04493T +$

$0.45525\varphi_M - 0.01014\varphi_{CNT} + 0.45150) + 0.08139 \tanh (-0.09280\gamma + 0.00407T - 1.75844\varphi_M -$

$0.22328\varphi_{CNT} + 1.44124) - 0.52171 \tanh (0.14031\gamma + 0.00052T - 4.39738\varphi_M - 0.00719\varphi_{CNT} +$

$3.30400) - 0.04611 \tanh (-0.06569\gamma + 0.00073T + 2.48100\varphi_M + 0.00205\varphi_{CNT} - 1.03603) + 0.08759$

$\tanh (0.08788\gamma - 0.00410T + 1.69327\varphi_M + 0.22057\varphi_{CNT} - 1.33532) + 0.00066 \tanh (-0.00508\gamma -$

$0.03150T + 1.26008\varphi_M + 0.43853\varphi_{CNT} + 0.55153) + 0.01716 \tanh (0.14865\gamma - 0.00045T -$

$0.98651\varphi_M + 0.25307\varphi_{CNT} - 0.85218) + 2.25789 \tanh (-0.06180\gamma + 0.000003T + 2.26987\varphi_M -$

$0.00222\varphi_{CNT} - 2.86749) - 1.08194 \tanh (-0.11371\gamma - 0.00017T + 3.66682\varphi_M + 0.02690\varphi_{CNT} -$

$3.01085) + 0.49907 \tanh (-0.48296\gamma - 0.00190T + 0.00935\varphi_M + 0.05003\varphi_{CNT} + 0.09833) - 0.13648$

$$\tanh (-0.02383\gamma - 0.03677T + 0.37656\varphi_M - 0.02106\varphi_{CNT} - 0.42817) + 0.70822 \tag{A.2}$$

443

References

445 [1] Omidi M, Farhadi M, Jafari M. A comprehensive review on double pipe heat exchangers.

446 Applied Thermal Engineering. 2017;110:1075-90.

447 [2] Ghani S, Gamaledin SMA, Rashwan MM, Atieh MA. Experimental investigation of double-

448 pipe heat exchangers in air conditioning applications. Energy and Buildings. 2018;158:801-11.

449 [3] Rashidi S, Eskandarian M, Mahian O, Poncet S. Combination of nanofluid and inserts for heat

450 transfer enhancement. Journal of Thermal Analysis and Calorimetry. 2018:1-24.

451 [4] Izadi M, Behzadmehr A, Shahmardan M. Effects of inclination angle on mixed convection heat

452 transfer of a nanofluid in a square cavity. International Journal for Computational Methods in

453 Engineering Science and Mechanics. 2015;16:11-21.

454 [5] Pramuanjaroenkij A, Tongkratoke A, Kakaç S. Numerical Study of Mixing Thermal

455 Conductivity Models for Nanofluid Heat Transfer Enhancement. Journal of Engineering Physics

456 and Thermophysics. 2018;91:104-14.

457 [6] Rashidi S, Karimi N, Mahian O, Esfahani JA. A concise review on the role of nanoparticles

458 upon the productivity of solar desalination systems. Journal of Thermal Analysis and Calorimetry.

459 2018:1-15.

460 [7] Mehryan S, Ghalambaz M, Izadi M. Conjugate natural convection of nanofluids inside an

461 enclosure filled by three layers of solid, porous medium and free nanofluid using Buongiorno's

462 and local thermal non-equilibrium models. Journal of Thermal Analysis and Calorimetry.1-21.

463 [8] Izadi M, Shahmardan M, Maghrebi MJ, Behzadmehr A. Numerical study of developed laminar

464 mixed convection of Al2O3/water nanofluid in an annulus. Chemical Engineering

465 Communications. 2013;200:878-94.

466   [9] Chol S, Estman J. Enhancing thermal conductivity of fluids with nanoparticles. ASME-

467   Publications-Fed. 1995;231:99-106.

468   [10] Rashidi S, Mahian O, Languri EM. Applications of nanofluids in condensing and evaporating

469   systems. Journal of Thermal Analysis and Calorimetry. 2018;131:2027-39.

470   [11] Rashidi S, Javadi P, Esfahani JA. Second law of thermodynamics analysis for nanofluid

471   turbulent flow inside a solar heater with the ribbed absorber plate. Journal of Thermal Analysis

472   and Calorimetry. 2018:1-13.

473   [12] Akbarzadeh M, Rashidi S, Karimi N, Omar N. First and second laws of thermodynamics

474   analysis of nanofluid flow inside a heat exchanger duct with wavy walls and a porous insert.

475   Journal of Thermal Analysis and Calorimetry. 2018:1-18.

476   [13] Rashidi S, Akbarzadeh M, Karimi N, Masoodi R. Combined effects of nanofluid and

477   transverse twisted-baffles on the flow structures, heat transfer and irreversibilities inside a square

478   duct–a numerical study. Applied Thermal Engineering. 2018;130:135-48.

479   [14] Shamsabadi H, Rashidi S, Esfahani JA. Entropy generation analysis for nanofluid flow inside

480   a duct equipped with porous baffles. Journal of Thermal Analysis and Calorimetry.1-11.

481   [15] Izadi M, Sinaei S, Mehryan S, Oztop HF, Abu-Hamdeh N. Natural convection of a nanofluid

482   between two eccentric cylinders saturated by porous material: Buongiorno's two phase model.

483   International Journal of Heat and Mass Transfer. 2018;127:67-75.

484   [16] Izadi M, Shahmardan M, Norouzi M, Rashidi A, Behzadmehr A. Cooling performance of a

485   nanofluid flow in a heat sink microchannel with axial conduction effect. Applied Physics A.

486   2014;117:1821-33.

487   [17] Izadi M, Behzadmehr A, Shahmardan MM. Effects of discrete source-sink arrangements on

488   mixed convection in a square cavity filled by nanofluid. Korean Journal of Chemical Engineering.

489   2014;31:12-9.

490   [18] Shakiba A, Vahedi K. Numerical analysis of magnetic field effects on hydro-thermal behavior

491   of a magnetic nanofluid in a double pipe heat exchanger. Journal of Magnetism and Magnetic

492   Materials. 2016;402:131-42.

493   [19] Azmi WH, Sharma KV, Mamat R, Najafi G, Mohamad MS. The enhancement of effective

494   thermal conductivity and effective dynamic viscosity of nanofluids – A review. Renewable and

495   Sustainable Energy Reviews. 2016;53:1046-58.

496   [20] Toghraie D, Chaharsoghi VA, Afrand M. Measurement of thermal conductivity of ZnO–

497   TiO2/EG hybrid nanofluid. Journal of Thermal Analysis and Calorimetry. 2016;125:527-35.

498   [21] Pryazhnikov MI, Minakov AV, Rudyak VY, Guzei DV. Thermal conductivity measurements

499   of nanofluids. International Journal of Heat and Mass Transfer. 2017;104:1275-82.

500   [22] Alirezaie A, Hajmohammad MH, Hassani Ahangar MR, Hemmat Esfe M. Price-performance

501   evaluation of thermal conductivity enhancement of nanofluids with different particle sizes.

502   Applied Thermal Engineering. 2018;128:373-80.

503   [23] Maddah H, Alizadeh M, Ghasemi N, Alwi SRW. Experimental study of Al2O3/water

504   nanofluid turbulent heat transfer enhancement in the horizontal double pipes fitted with modified

505   twisted tapes. International Journal of Heat and Mass Transfer. 2014;78:1042-54.

506   [24] Mousavi SV, Sheikholeslami M, Gerdroodbary MB. The Influence of magnetic field on heat

507   transfer of magnetic nanofluid in a sinusoidal double pipe heat exchanger. Chemical Engineering

508   Research and Design. 2016;113:112-24.

509   [25] Saeedan M, Nazar ARS, Abbasi Y, Karimi R. CFD Investigation and neutral network

510   modeling of heat transfer and pressure drop of nanofluids in double pipe helically baffled heat

511   exchanger with a 3-D fined tube. Applied Thermal Engineering. 2016;100:721-9.

512   [26] Sarafraz M, Hormozi F, Nikkhah V. Thermal performance of a counter-current double pipe

513   heat exchanger working with COOH-CNT/water nanofluids. Experimental Thermal and Fluid

514   Science. 2016;78:41-9.

515   [27] Kumar NR, Bhramara P, Sundar LS, Singh MK, Sousa AC. Heat transfer, friction factor and

516   effectiveness of Fe3O4 nanofluid flow in an inner tube of double pipe U-bend heat exchanger with

517   and without longitudinal strip inserts. Experimental Thermal and Fluid Science. 2017;85:331-43.

518   [28] Hussein AM. Thermal performance and thermal properties of hybrid nanofluid laminar flow

519   in a double pipe heat exchanger. Experimental Thermal and Fluid Science. 2017;88:37-45.

520   [29] Shirvan KM, Mamourian M, Mirzakhanlari S, Ellahi R. Numerical investigation of heat

521   exchanger effectiveness in a double pipe heat exchanger filled with nanofluid: a sensitivity analysis

522   by response surface methodology. Powder Technology. 2017;313:99-111.

523   [30] Afrand M, Toghraie D, Ruhani B. Effects of temperature and nanoparticles concentration on

524   rheological behavior of Fe3O4–Ag/EG hybrid nanofluid: an experimental study. Experimental

525   Thermal and Fluid Science. 2016;77:38-44.

526   [31] Rostamian SH, Biglari M, Saedodin S, Esfe MH. An inspection of thermal conductivity of

527   CuO-SWCNTs hybrid nanofluid versus temperature and concentration using experimental data,

528   ANN modeling and new correlation. Journal of Molecular Liquids. 2017;231:364-9.

529   [32] Esfe MH, Alirezaie A, Rejvani M. An applicable study on the thermal conductivity of

530   SWCNT-MgO hybrid nanofluid and price-performance analysis for energy management. Applied

531   Thermal Engineering. 2017;111:1202-10.

[33] Esfahani NN, Toghraie D, Afrand M. A new correlation for predicting the thermal conductivity of ZnO–Ag (50%–50%)/water hybrid nanofluid: An experimental study. Powder Technology. 2018;323:367-73.

[34] Moldoveanu GM, Huminic G, Minea AA, Huminic A. Experimental study on thermal conductivity of stabilized Al2O3 and SiO2 nanofluids and their hybrid. International Journal of Heat and Mass Transfer. 2018;127:450-7.

[35] Karimi A, Afrand M. Numerical study on thermal performance of an air-cooled heat exchanger: Effects of hybrid nanofluid, pipe arrangement and cross section. Energy Conversion and Management. 2018;164:615-28.

[36] Izadi M, Mohebbi R, Karimi D, Sheremet MA. Numerical simulation of natural convection heat transfer inside a$\perp$ shaped cavity filled by a MWCNT-Fe3O4/water hybrid nanofluids using LBM. Chemical Engineering and Processing-Process Intensification. 2018;125:56-66.

[37] Esfe MH, Esfandeh S, Afrand M, Rejvani M, Rostamian SH. Experimental evaluation, new correlation proposing and ANN modeling of thermal properties of EG based hybrid nanofluid containing ZnO-DWCNT nanoparticles for internal combustion engines applications. Applied Thermal Engineering. 2018;133:452-63.

[38] Theres Baby T, Sundara R. Surfactant free magnetic nanofluids based on core-shell type nanoparticle decorated multiwalled carbon nanotubes. Journal of Applied Physics. 2011;110:064325.

[39] Felicia LJ, Philip J. Magnetorheological properties of a magnetic nanofluid with dispersed carbon nanotubes. Physical Review E. 2014;89:022310.

553   [40] Sundar LS, Singh MK, Sousa AC. Enhanced heat transfer and friction factor of MWCNT–

554   Fe3O4/water hybrid nanofluids. International Communications in Heat and Mass Transfer.

555   2014;52:73-83.

556   [41] Shahsavar A, Saghafian M, Salimpour M, Shafii M. Experimental investigation on laminar

557   forced convective heat transfer of ferrofluid loaded with carbon nanotubes under constant and

558   alternating magnetic fields. Experimental Thermal and Fluid Science. 2016;76:1-11.

559   [42] Harandi SS, Karimipour A, Afrand M, Akbari M, D'Orazio A. An experimental study on

560   thermal conductivity of F-MWCNTs–Fe3O4/EG hybrid nanofluid: effects of temperature and

561   concentration. International Communications in Heat and Mass Transfer. 2016;76:171-7.

562   [43] Moradi H, Bazooyar B, Etemad SG, Moheb A. Influence of the geometry of cylindrical

563   enclosure on natural convection heat transfer of Newtonian nanofluids. Chemical Engineering

564   Research and Design. 2015;94:673-80.

565   [44] Hojjat M. Modeling heat transfer of non-Newtonian nanofluids using hybrid ANN-

566   Metaheuristic optimization algorithm. Journal of Particle Science & Technology. 2018;3:233-41.

567   [45] Sandeep N, Malvandi A. Enhanced heat transfer in liquid thin film flow of non-Newtonian

568   nanofluids embedded with graphene nanoparticles. Advanced Powder Technology. 2016;27:2448-

569   56.

570   [46] Akbari OA, Toghraie D, Karimipour A, Marzban A, Ahmadi GR. The effect of velocity and

571   dimension of solid nanoparticles on heat transfer in non-Newtonian nanofluid. Physica E: Low-

572   dimensional Systems and Nanostructures. 2017;86:68-75.

573   [47] Singh AK, Kishore N. Laminar Mixed Convection of Non-Newtonian Nanofluids Flowing

574   Vertically Upward Across a Confined Circular Cylinder. Journal of Thermal Science and

575   Engineering Applications. 2018;10:041012--14.

576 [48] Shahsavar A, Saghafian M, Salimpour M, Shafii M. Effect of temperature and concentration

577 on thermal conductivity and viscosity of ferrofluid loaded with carbon nanotubes. Heat and Mass

578 Transfer. 2016;52:2293-301.

579 [49] Berger P, Adelman NB, Beckman KJ, Campbell DJ, Ellis AB, Lisensky GC. Preparation and

580 properties of an aqueous ferrofluid. Journal of Chemical Education. 1999;76:943.

581 [50] Garg P, Alvarado JL, Marsh C, Carlson TA, Kessler DA, Annamalai K. An experimental

582 study on the effect of ultrasonication on viscosity and heat transfer performance of multi-wall

583 carbon nanotube-based aqueous nanofluids. International Journal of Heat and Mass Transfer.

584 2009;52:5090-101.

585 [51] Shahsavar A, Bahiraei M. Experimental investigation and modeling of thermal conductivity

586 and viscosity for non-Newtonian hybrid nanofluid containing coated CNT/Fe3O4 nanoparticles.

587 Powder Technology. 2017;318:441-50.

588 [52] Mohammed HA, Narrein K. Thermal and hydraulic characteristics of nanofluid flow in a

589 helically coiled tube heat exchanger. International Communications in Heat and Mass Transfer.

590 2012;39:1375-83.

591 [53] Duangthongsuk W, Wongwises S. An experimental study on the heat transfer performance

592 and pressure drop of TiO2-water nanofluids flowing under a turbulent flow regime. International

593 Journal of Heat and Mass Transfer. 2010;53:334-44.

594 [54] Lienhard JH. A heat transfer textbook: Courier Corporation; 2013.

595